Formation energies, electronic structure, and hyperfine fields of chalcogen point defects and defect pairs in silicon

H. Overhof
Universität Paderborn, Warburger Strasse 100, D-4790 Paderborn, Germany

M.Scheffler
Fritz-Haber-Institut der Max-Planck-Gesellschaft, Faradayweg 4-6, D-1000 Berlin 33, Germany

C. M. Weinert
Heinrich-Hertz Institut, Einsteinufer 37, D-1000 Berlin 12, Germany
(Received 10 October 1990; revised manuscript received 20 March 1991)

The electronic structure of substitutional and interstitial S, Se, and Te point defects and of defect pairs is investigated by *ab initio* total-energy calculations. The results show that under normal conditions the chalcogen point defects are preferentially built in as substitutional atoms. However, interstitial S point defects cannot be excluded for n-type material. According to our calculations, the formation energy (without Jahn-Teller distortion) is 1 eV higher than for the substitutional S point defect. Stable pairs are formed in n-type material for nearest-neighbor substitutional S and Se atoms. For Te pairs the formation energy is always larger than that for two isolated point defects. Lattice relaxation (which is ignored in our calculation) could lower this value in order to allow for stable Te pairs. Pairs of interstitial chalcogen defects and also mixed pairs of interstitial and substitutional chalcogen would also be stable if there was a sufficient concentration of interstitials. We find that more distant pairs can also be stable for S and Se whereas for Te pairs they are unlikely. We calculate the matrix elements of the hyperfine interaction with the impurity nuclei and also the ligand hyperfine matrix elements with several Si ligands and for several different paramagnetic configurations of the point defects and the pairs. We find good agreement between the experimental data and our results for those configurations that have been found to be stable according to total-energy calculations. We also find that next-nearest-neighbor pairs can be stable and speculate if such pairs can be identified with the chalcogen X center.

I. INTRODUCTION

A major task in semiconductor research is the identification of the chemical nature and atomic structure of defects, in particular, of defects that exist in several modifications in a given crystal. Among the defects that form deep levels in silicon the chalcogens S, Se, and Te have been the subject of many detailed studies, see, e.g., Wagner *et al.*[1] for a review.

In this paper we theoretically investigate the electronic structures, total energies, and hyperfine fields of the S, Se, and Te isolated point defects and of the D_{3d} and C_{3v} symmetry pairs. The results are compared with experimental data, which give a wealth of information about the properties of deep states: From infrared absorption[2-6] and from deep-level transient spectroscopy (DLTS) experiments[7] the position of the levels in the gap are known accurately. Electron paramagnetic resonance[8,9] (EPR) and electron nuclear double resonance[8,10-14] (ENDOR) experiments result in detailed information about the point-group symmetry of the defect. In particular the ENDOR experiments give detailed information involving the shape of the spin-density distribution at the impurity nucleus and also at several close and more distant host ligand nuclei. Unfortunately, this information cannot be used directly to map the deep-level wave function in real space. In fact, it is not even possible to discriminate (without introducing significant theoretical assumptions) a substitutional site for the point defect from an interstitial site since both have tetrahedral symmetry in the diamond lattice.

A further interesting topic for which there is little experimental information is the structure of impurity pairs. Again from ENDOR data one can deduce the symmetry of the pair, but that does not identify the distance between the nuclei of the pair (and for the case of pairs with D_{3d} symmetry again does not discriminate a pair formed by two impurities on interstitial sites from a pair of two impurities on substitutional sites). Little if any information can be derived from experimental data about the formation energy of pairs, in particular as this quantity depends sensitively upon the position of the Fermi energy.

Here theoretical total-energy calculations are powerful tools that allow the calculation of pair formation energies, of the energy of the deep levels, and also of the hy-

perfine and ligand hyperfine interaction matrix elements. We shall present in this paper a detailed investigation of the properties of point defects and pairs in all charge states and in different atomic configurations. In particular we discuss the stability of S and Se point defects and of pairs of S and Se. We also calculate the paramagnetic properties of these impurity configurations which can be compared directly with experimental hyperfine data. The different contributions to the spin density that arise from the spin polarization of the core states, the spin polarization of the valence-band states, and the contribution from the single-particle wave function of the state in the gap are discussed in some detail. We find that at the ligands the polarization of the valence band states can be quite significant. The single-particle linear combination of atomic orbitals (LCAO) scheme[15–19] which is frequently used for the interpretation of experimental data does not take this valence-band polarization explicitly into account and can therefore lead to an erroneous description of the bonding properties at the ligands when forced to reproduce the experimental EPR and ENDOR data.

II. COMPUTATIONAL

Ab initio self-consistent electronic structure calculations for defects in solids can be performed efficiently using the Green-function approach. This approach has the advantage that the problem separates into two parts, the calculation of the Green function for the perfect crystal, G_0, and the solution of a Dyson equation for the Green function G of the crystal with the impurity (or impurity complex). In this scheme the Green function G_0 has to be calculated self-consistently for an infinite perfect crystal in a first step. Exchange and correlation are treated in the local-spin-density approximation (LSDA) of the spin-density functional theory[20] (DFT) (see also Ref. 21). In a second step the Green function G for the infinite crystal with a point defect (or a defect complex) is obtained by a solution of Dyson's equation

$$G = G_0 + G_0 \, \Delta V \, G \, . \tag{1}$$

Here ΔV is the potential which describes the perturbation caused by the impurity. Dyson's equation has to be solved self-consistently using again the DFT-LSDA method.

In this paper we shall be interested particularly in the paramagnetic properties of defects which are determined predominantly by the spin densities near the nuclei of the defect and its ligands. We therefore have used the linear muffin-tin orbital method in the atomic-sphere approximation (LMTO-ASA).[22] In the LMTO-ASA method the crystal is divided into overlapping spheres with spherical symmetrical potentials for which the Kohn-Sham equation is solved directly. The solution of Dyson's equation is considerably simplified by the fact that the potential ΔV is localized in a rather small region in space around the impurity site only, although the wave functions of the resulting states will extend over a significantly larger spatial region. A self-consistent solution of Dyson's equation can therefore be obtained treating a rather small number of atomic spheres around the impurity.

The use of the ASA unfortunately does not allow us to treat the effect of lattice relaxation around the impurity. The effect of this relaxation has been shown[23] to be small for Si:S and Si:Se. For Si:Te, however, the geometrical misfit of the larger impurity atom may cause important uncertainties. We shall in the main part of the paper restrict our attention to defects that exhibit T_d point-group symmetry and to pairs of D_{3d} and C_{3v} symmetry. The perturbed region will be constructed in such a way that the point-group symmetry of the defect is retained which allows the use of symmetry-adapted muffin-tin orbitals.

A. The resonance problem

It is well known that the single-particle band gap of the DFT-LSDA calculations for silicon is too small by about 0.5 eV if compared to the experimental band gap. In the case of chalcogen point defects and defect pairs this deficiency has the consequence that the defect-induced gap state turns out to be a resonance near the bottom of the conduction band. For the paramagnetic isolated point defects and defect pairs of the chalcogens this gap state is singly occupied. This is modeled in our calculation by an occupation of the resonance state with one unpaired electron. The change of the resulting density-of-states distribution with respect to a perfect crystal for the resonance is shown in Fig. 1 for Se_{Si}^{+}.

In order to obtain a quantitative estimate of the effect of the resonance we have performed non-self-consistent calculations: the self-consistent potential for the perturbed region containing the impurity and the next 16 Si ligands was modified by the addition of a small constant potential δV. This potential is used to force the

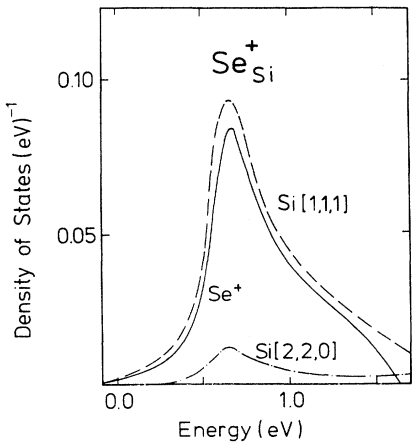

FIG. 1. Induced density of states for the a_1 resonance state of Se_{Si}^{+} projected into the Se^{+} sphere (solid line), into the Si(1,1,1) ligand sphere (dashed line), and into a Si(2,2,0) ligand sphere (dash-dotted line).

deep level down into the band gap thereby altering the localization of the resonance state. We find that for S_{Si}^{+} and Se_{Si}^{+} a potential $\delta V = -0.15$ eV is sufficient and leads to an increase of the electron density of the resonance in the ASA shells of the perturbed region that amounts to less than 10%. For Te_{Si}^{+}, on the other hand, the resonance is found to be significantly higher in the conduction band than for S_{Si}^{+} and Se_{Si}^{+}. In this case the value of δV required to shift the resonance into the gap is larger by a factor of 8. This larger shift is accompanied by an increase of the electron density of the resonance in the Te ASA sphere and also in the nearest-neighbor ligand spheres by more than a factor of 2.

We thus find that in the case of S_{Si}^{+} and Se_{Si}^{+} it is permissible to identify the resonance with the defect-induced localized state. We note that the error in the electron density (and also in the spin density, etc.) arising from the resonance nature of the induced state is expected to be below 10%. For Te_{Si}^{+} we expect larger errors. In the remainder of this paper we shall address the resonance as "deep state" and its energy as the "deep level." All calculated quantities quoted will be derived self-consistently from the deep-state resonance without any correction by an additional potential δV.

B. Hyperfine interaction

In electron paramagnetic resonance (EPR) and electron nuclear double resonance (ENDOR) experiments the hyperfine interaction (HFI) matrix elements of a paramagnetic impurity with the impurity nucleus can be determined if there are isotopes with nonzero nuclear spin for the impurity. From the experimental data the point-group symmetry of the defect site can be obtained directly. A distinction between a tetrahedral substitutional site and a tetrahedral interstitial site, however, is not possible directly.[24] Besides the interaction with the impurity nucleus the ENDOR data can provide the ligand HFI matrix elements with the magnetic host crystal nuclei at different ligand positions with respect to the impurity. Again a careful analysis of the angular dependence of the ENDOR data provides the information about the symmetry of the "shell" of equivalent ligands that are transformed into each other by the operations of the symmetry group of the defect cluster. This means that one obtains directly the point-group symmetry of the shell of distance vectors between the paramagnetic impurity and the ligand nuclei but not the length of these vectors. There is no simple way to estimate these distances. In particular, it is in general not correct to assign the smallest distance vectors to the largest HFI matrix elements as is sometimes assumed in experimental analyses. It should be noted that even for shallow donors in silicon[25,26] it is known that the ligand hyperfine matrix elements for the nearest-neighbor ligand is much smaller than that for several more distant ligands. For donor impurities that are described by the effective-mass approximation (EMA) the matrix elements depend in an oscillatory way on the distance vector from the impurity site. This is due to the fact that in Si there are several inequivalent conduction-band minima.[27] For deep impurities the EMA does not hold but nevertheless the HFI matrix elements will in general depend in an oscillatory way on the distance from the impurity site.

The isotropic hyperfine interaction (also called the Fermi contact term) for an electron with gyromagnetic ratio g_e interacting with a nucleus at the site $\mathbf{R}_N$ with gyromagnetic ratio g_N is given by

$$a_N = \tfrac{2}{3}\,\mu_0\, g_e\, g_N\, \mu_N\, m(\mathbf{R}_N)\ , \tag{2}$$

where μ_0 is the susceptibility constant and μ_N is the nuclear magneton. The magnetization density at the nuclear site $\mathbf{R}_N$ is the product of Bohr's magneton μ_B and the difference $m(\mathbf{r})$ between the electron spin densities of up and down spins, $n_\uparrow$ and $n_\downarrow$, respectively,

$$m(\mathbf{r}) = \mu_B\,[n_\uparrow(\mathbf{r}) - n_\downarrow(\mathbf{r})]. \tag{3}$$

$m(\mathbf{r})$ can be analyzed in terms of three different contributions. The first contribution arises from the paramagnetic spin of the single-particle wave function describing the deep state. This contribution actuates the magnetization of other states. As a consequence of this deep-level wave function we will have a spin-dependent modification of the valence-band states, i.e., a spin polarization of the valence states, and also a spin polarization of the impurity and ligand core states.

It should be noted that for the computation of particle and of spin densities in the nuclear region of atoms it is important to take relativistic effects into account, at least by using a scalar relativistic wave equation (see, e.g., Ref. 28). In the Mössbauer spectroscopy (see, e.g., Refs. 29 and 30) it is customary to correct particle densities obtained using a nonrelativistic calculation by a function $S'(Z)$, which can be shown to be a good approximation to relativistic particle densities. $S'(Z)$ depends on the nuclear charge only and amounts to 1.12 for S, 1.54 for Se, and 2.61 for Te. For the contact interaction the same correction must not be used because in a relativistic theory[31,32] the magnetization density is not to be averaged over the nuclear volume but rather over a sphere with diameter equal to the Thomas radius $r_{\rm th} = Ze^2/(2mc^2)$. For test purposes we have performed nonrelativistic calculations and obtained isotropic HFI constants that are smaller than the corresponding results of a relativistic calculation by a factor of 1.02 for the HFI at Si nuclei, 1.03 at S, 1.16 at Se, and 1.45 at Te nuclei, respectively.

The anisotropic (dipolar) HFI is given by an integral over the magnetization density over all space

$$(b_N)_{i,j} = \frac{\mu_0}{8\pi}\, g_e\, g_N\, \mu_N \int \frac{3x_i x_j - r^2\delta_{i,j}}{r^5}\, m(\mathbf{r}+\mathbf{R}_N)\, d^3r\ . \tag{4}$$

The integrand is strongly peaked at the nucleus and, therefore, it is sufficient in practically all cases to per-

form the integration over the central ASA sphere and to approximate the contributions from the other spheres replacing the spin distribution in each of these spheres by point dipoles with a dipole moment appropriate for the integrated spin density in the spheres. For the computation of the anisotropic part of the HFI, relativistic effects turned out to be of minor importance. The anisotropic hyperfine tensor can be diagonalized into the form

$$(b_N)_{i,j} = \begin{pmatrix} b-b' & 0 & 0 \\ 0 & b+b' & 0 \\ 0 & 0 & -2b \end{pmatrix} . \quad (5)$$

We shall present in the following the dipolar constant b exclusively and do not attempt to calculate b'. For a nucleus in the center of the perturbed region b' is zero due to the symmetry. For nuclei that are not on a threefold-symmetry axis of the perturbed region (and only for these nuclei b' will be nonzero) we cannot even calculate the contributions of all nearest neighbors because our perturbed region is too small for this purpose. As a consequence we shall present also the calculated data for b in parentheses in these cases.

In the following we denote by a_l and b_l the hyperfine matrix elements which are calculated from the spin density of the single-particle density of the deep state alone. By $a_{\rm tot}$ and $b_{\rm tot}$ we denote the hyperfine matrix elements which are calculated from the total spin densities which includes contributions from the deep state, the valence band, and from the core states. The spin polarization of the core states was taken into account in each step of the self-consistent cycle using the potential derived from the solution of Dyson's equation in an atomic Dirac-LSDA calculation.

III. RESULTS

A. Isolated impurity atoms

For the total-energy computation of the substitutional chalcogen point defects we have used a perturbed region that consists of the impurity site, the four (1,1,1) nearest-neighbor silicon sites and the twelve (2,2,0) next-nearest silicon sites (we label the complete shell of neighbors by one representative and denote distance vectors in units of $d = a/4$ where a is the lattice constant). Outside this region ΔV would be small and is therefore set to zero in the calculation. For a proper fill factor of the crystal we have also included "empty" spheres at the tetrahedral interstitial sites. This gives us a total of 27 atomic spheres. We have in addition calculated the spin densities, etc., for the Si(3,1,$\bar{1}$) and the Si(3,3,$\bar{3}$) sites. In these calculations the impurity site was not in the center of the perturbed region. As a consequence the symmetry of the perturbed region was C_{3v} instead of T_d. These calculations are, therefore, less accurate. Due to computational limitations we have not been able to include more distant ligands into our calculation.

The distribution of the induced density of states for S_{Si}^{+} that transforms according to the irreducible representations A_1 and T_2 is shown in Fig. 2. The induced densities of states are identical to those presented earlier[33] and will be discussed in more detail in connection with the results for the pairs.

In the experiment the paramagnetic deep states of S_{Si}^{+} and Se_{Si}^{+} are at midgap, thus energetically these states are very deep. This does not mean, however, that the spin density of these states is localized within a few unit cells around the impurity site. This is demonstrated in Table I where we list the s, p, and d components of the charge densities obtained from the single-particle wave function and projected into the different ASA spheres. According to our calculations only 4.0% of an elementary charge is located within the S^{+} ASA sphere, 4.3% is within each of the four Si(1,1,1) ligands, 0.5% in each of the twelve Si(2,2,0) ligands, while 0.8% is found in each of the ten interstitial spheres. The sphere that contains the chalcogen atom and its nearest and next-nearest Si ligands, therefore, encloses only 35% of the total spin of this antibonding a_1 state. The corresponding bonding a_1 state is a hyperdeep resonance state within the valence band. The a_1 state below the valence band (see Fig. 2) is essentially an s state pulled down from the valence band. Here 77% of the particle density is found within the chalcogen atomic sphere while the remaining particle density is located predominantly at the nearest Si ligands.

1. Total energies

A plot of the induced density of states for the a_1 resonance level of Se_{Si}^{+} is shown in Fig. 1. The resonance has a characteristic asymmetry. We will take the maxi-

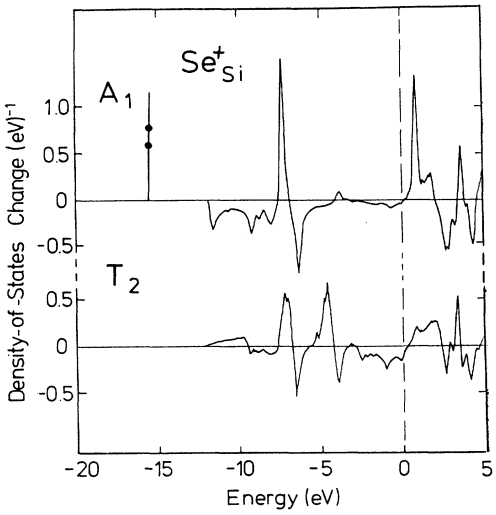

FIG. 2. Induced density of states symmetry for the Se_{Si}^{+} point defect transforming according to the A_1 representation (upper panel) and to the T_2 representation (lower panel).

TABLE I. Occupation of the different partial waves of the deep-level wave function for the S_{Si}^{+} and the Se_{Si}^{+} point defects and for the NN and NNN $(S_{Si}\text{-}S_{Si})^{+}$ and $(Se_{Si}\text{-}Se_{Si})^{+}$ defect pairs.

Shell	s	p	d	s	p	d
		S_{Si}^{+}			Se_{Si}^{+}	
chalcogen	0.0401	0.0	0.0	0.0310	0.0	0.0
Si(1,1,1)	0.0020	0.040	0.0042	0.0021	0.0307	0.0038
Si(2,2,0)	<0.0001	0.0009	0.0042	<0.0001	0.0003	0.0038
Si(3,1,$\bar{1}$)	0.0035	0.0015	0.0010	0.0030	0.0009	0.0007
Si(3,3,$\bar{3}$)	0.0007	<0.0001	<0.0001	0.0006	<0.0001	< 0.0001
		$(S_{Si}\text{-}S_{Si})^{+}$ NN pair			$(Se_{Si}\text{-}Se_{Si})^{+}$ NN pair	
chalcogen	0.0139	0.0106	0.0041	0.0108	0.0092	0.0030
Si(1,1,1)	0.0009	0.0151	0.0023	0.0009	0.0129	0.0024
		$(S_{Si}\text{-}S_{Si})^{+}$ NNN pair			$(Se_{Si}\text{-}Se_{Si})^{+}$ NNN pair	
chalcogen	0.0127	0.0113	0.0042	0.0091	0.0023	0.0031
Si(1,1,1)	<0.0001	0.0030	0.0045	< 0.0001	0.0025	0.0035
		$(S_{Si}\text{-}S_{Si})^{+++}$ NNN pair			$(Se_{Si}\text{-}Se_{Si})^{+++}$ NNN pair	
chalcogen	0.0175	0.0082	0.0013	0.0161	0.0075	0.0010
Si(1,1,1)	<0.0001	0.0021	0.0020	< 0.0001	0.00163	0.0020

mum of this resonance as the single-particle energy of the deep level. The single-particle energy of a single-particle wave function cannot be compared with an energy level observed by DLTS or optical experiments. For such comparison it is necessary to calculate electron removal energies either from total-energy differences or from the corresponding transition states. It should also be noted that DLTS and optical data are not necessarily giving the same deep-level energies, because they differ in the contribution of the lattice relaxation which takes place upon relaxation. However, calculations by Scheffler[23] for S in Si predicted that this Franck-Condon shift is very small (≤ 0.05 eV). It is not known, however, how this theoretical number compares to experimental results. From our calculations we obtain the formation energy $\Delta E_{\rm tot}$. This is the difference between the total energies of the system "crystal perturbed by an impurity" and the system "isolated atom plus a perfect crystal." For charged impurities this difference depends on the position of the Fermi energy.[34,35] This energy has to be corrected because in our calculation the Coulomb tail of the self-consistent field (SCF) potential of a charged impurity is cut off outside the perturbed region. From perturbation theory we estimate that this treatment requires a correction of the SCF calculation of U by $0.1n$ eV, where n is the impurity charge state. We show in Figs. 3(a) and 4(a) the calculated $\Delta E_{\rm tot}$ results for substitutional sulfur and selenium point defects. For each charge state we obtain a different straight line. The energies at which two lines intersect are the removal energies for an electron in this state: If the Fermi energy is at the removal energy there is no energetic difference between the two corresponding charge states. We observe a difference between the $E^{++/+}$ and the $E^{+/0}$ states that amounts to 0.20 eV for S and to 0.18 eV for Se which is to be identified with the electronic correlation energy U. We list in Table II the energies of the deep states in comparison with experimental data. We find a satisfactory agreement for S_{Si} and Se_{Si}.

In agreement with the calculations of Beeler *et al.*[33] we find for tetrahedral *interstitial* Se and Te point defects that the calculated $\Delta E_{\rm tot}$ is by several eV above the value obtained for the substitutional configuration. We therefore conclude that in thermal equilibrium there will be no significant concentration of interstitials of these atoms. For sulfur interstitials the situation is less clear. We find that for n-type silicon crystals the total energy for a $S_{\rm int}^{--}$ impurity is by about 1.4 eV above the total energy of a S_{Si}^{0} impurity. The state in the gap for the interstitial chalcogen impurity transforms according to the t_2 representation and, therefore, we expect a Jahn-Teller distortion (see, e.g., Ref. 36). Such a distortion will lower the total energy of the defect. Therefore, we cannot exclude that at least for n-type material a calculation that includes the structural relaxation could lead to a certain fraction of stable or metastable interstitial sulfur point defects.

2. *Hyperfine interaction matrix elements*

In Table III we compare our results for the HFI constants with experimental data taken from Refs. 8, 24, and from 11. As mentioned above it is not possible to determine the distance between the impurity site and the ligand nuclei from the experimental magnetic resonance data alone. The symmetry of the shell of ligand nuclei at equivalent positions with respect to the impurity site can be safely identified. We compare our calculated data for which of course the distance vectors are known with those experimental data for a given symmetry type for which the contact interactions are largest.

From Table III we find good agreement between our calculated HFI constants and the experimentally deter-

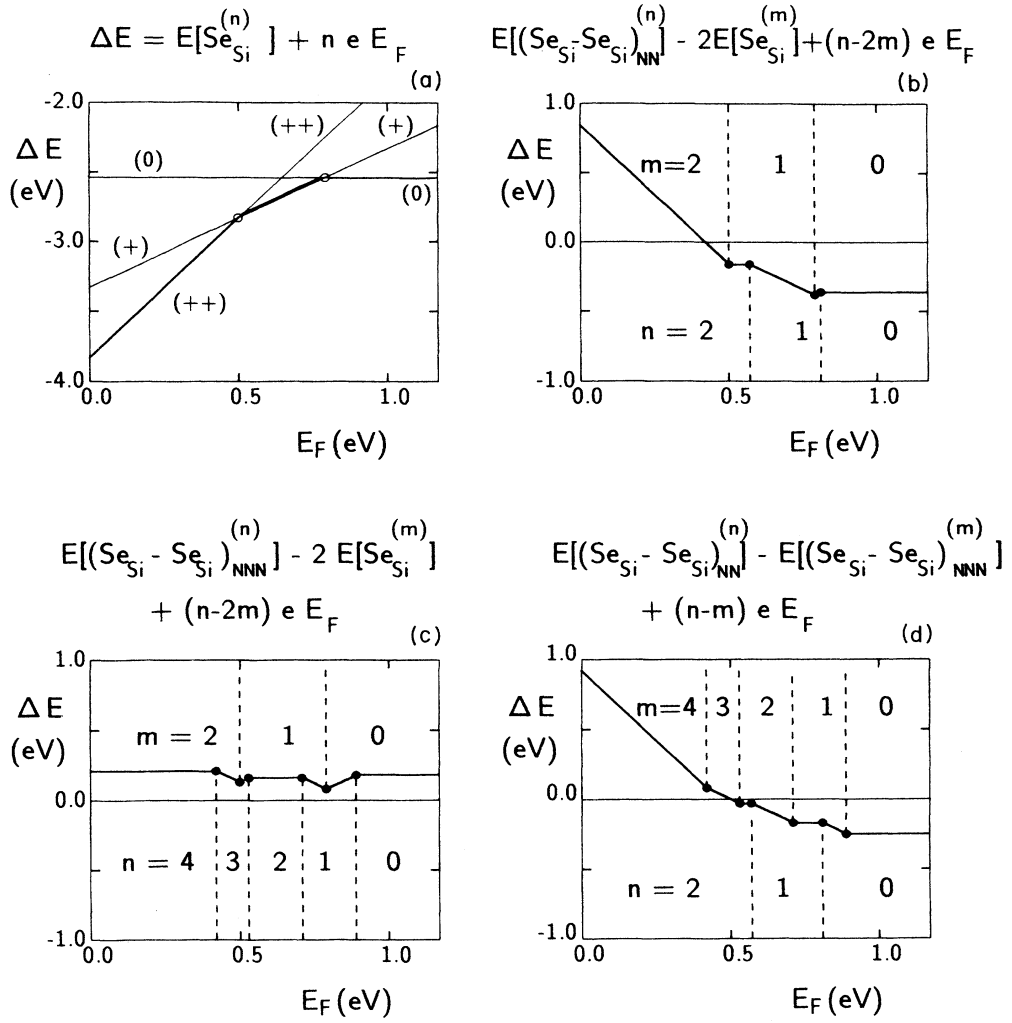

FIG. 3. Formation energy of substitutional S defect in different configurations and charge states as a function of the Fermi energy: (a) isolated point defect; (b) difference between a NN pair and two point defects; (c) difference between a NNN pair and two point defects; and (d) difference between a NN and a NNN pair. The zero of the energy scale in (a) refers to the case of an isolated S atom.

TABLE II. Calculated electron removal energies for deep states (in eV) with respect to the valence-band edge compared with experimental data (Ref. 6 for S and Se, Ref. 10 for Te point defects, and Ref. 1 for the Te pair).

Charge state	This work	Expt.	This work	Expt.	This work	Expt.
point defect						
+/0	0.82	0.852	0.79	0.863	0.89	0.97
++/+	0.52	0.556	0.50	0.577	0.75	0.716
SS NN pair						
+/0	0.90	0.982	0.81	0.964	0.90	1.016
++/+	0.56	0.799	0.57	0.78	0.63	
SS NNN pair						
+/0	0.99		0.89		1.09	
++/+	0.87		0.71		0.95	
+++/++	0.43		0.53		0.68	
++++/+++	0.25		0.42		0.54	

mined data for the contact interaction at the S^+ and Se^+ nuclei. The agreement between experimental data and our theoretical values is rather poor for the data at the Te^+ nucleus. This was to be expected from the fact that in the case of Te_{Si}^+ the resonance is shifted farther into the conduction band and that lattice relaxation will modify the wave functions significantly (see the discussion of this point in Ref. 37). Therefore it is not surprising that for the ligands in the Te_{Si}^+ system the agreement between theory and experiment is even worse.

The different contributions to the HFI matrix elements for the S_{Si}^+ and the Se_{Si}^+ point defects are summarized in Table IV. For the contact HFI with the impurity nuclei we find that the contribution from the deep level, a_l, is essentially identical with a_{tot}, with only small contributions from the valence and core polarization. For the HFI with the ligands, however, the inclusion of the valence-band and core polarization effects can be very important. The contribution of the valence-band polarization for the nearest-neighbor ligand is about the same as the contribution of the single-particle wave function. For the next-nearest neighbor almost the entire contact HFI term is made up of valence-band contributions.[38,39] This has the effect that the oscillations of the single-particle wave function which has a node at the next-nearest ligand site are less prominent in the HFI contact terms. The contribution of the core states is negative for all Si ligands and is of importance only for the Si(1,1,1) ligand, for all the other Si ligands the effect of the core polarization is small.

Inspection of Table I shows that the single-particle wave function at all Si ligands is essentially p type with

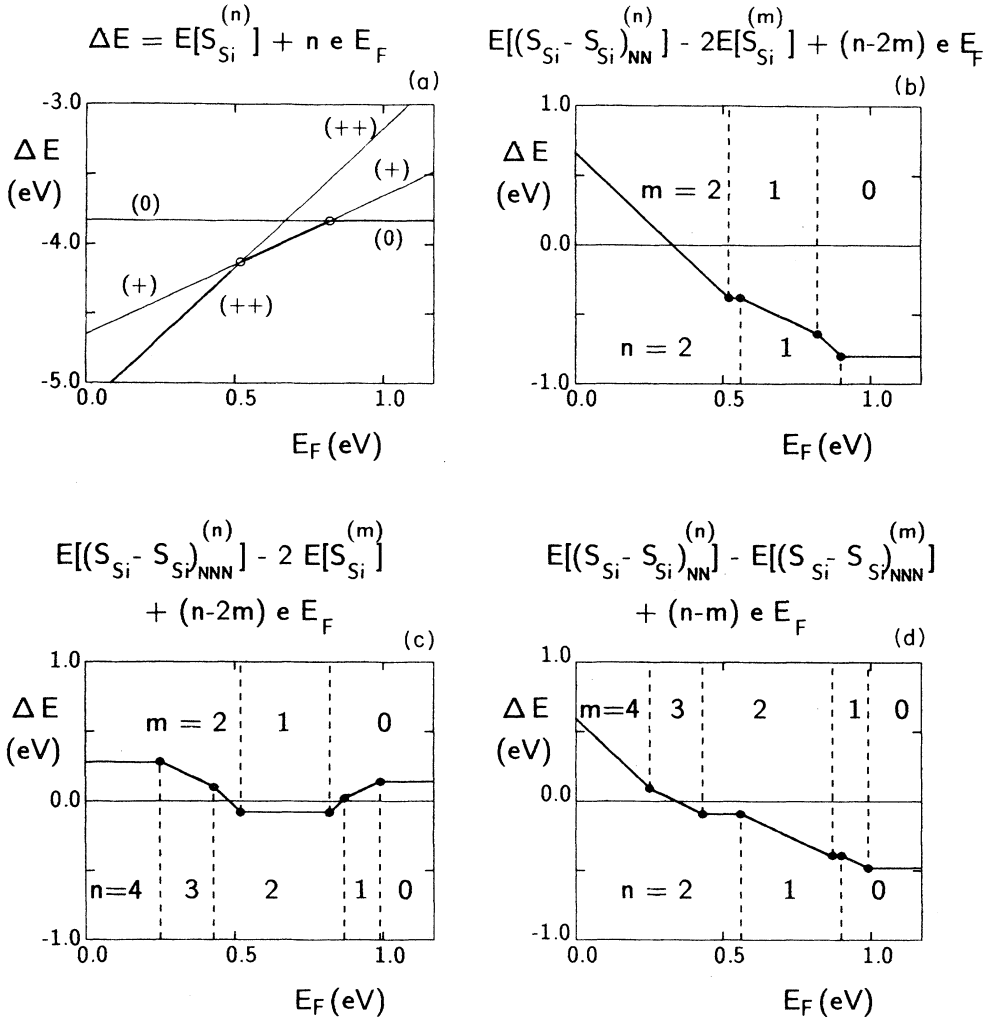

FIG. 4. Formation energy of substitutional Se defect clusters in different configurations and charge states as a function of the Fermi energy: (a) isolated point defect; (b) difference between a NN pair and two point defects; (c) difference between a NNN pair and two point defects; and (d) difference between a NN and a NNN pair. The zero of the energy scale in (a) refers to the case of an isolated S atom.

TABLE III. Comparison of the calculated and experimental hyperfine data for isolated substitutional chalcogen impurities (in MHz). a_l and b_l are calculated from the single-particle wave function of the deep level, while a_{tot} and b_{tot} are obtained from a calculation that takes into account the polarization of the valence band and core states also. The largest experimental contact interactions compatible with the symmetry of the shells are listed as a_{expt} and b_{expt}. Experimental data are taken from Ref. 8 for Si:S, from Ref. 11 for Si:Se, and from Ref. 24 for Si:Te.

Ligand	a_l	a_{tot}	a_{expt}	b_l	b_{tot}	b_{expt}
S^+_{Si}						
S^+	239.3	240.5	312.4	0.0	0.0	0.0
Si(1,1,1)	21.1	31.9	30.7	7.9	9.05	12.0
Si(2,2,0)	< 0.001	5.64	8.94	0.17	(0.28)	0.47
Si(3,1,$\bar{1}$)	3.0	3.11	3.84	0.45	(0.48)	0.42
			4.77			0.03
Si(3,3,$\bar{3}$)	6.0	6.2	9.00	<0.001	(0.05)	0.62
Se^+_{Si}						
Se^+	1176	1208	1658	0.0	0.0	0.0
Si(1,1,1)	15.6	25.4	28.9	7.1	8.1	12.5
Si(2,2,0)	< 0.001	5.29	7.54	0.01	(0.26)	0.52
Si(3,1,$\bar{1}$)	2.66	2.75	3.87	0.44	(0.54)	0.45
			4.27			0.11
			3.17			0.07
Si(3,3,$\bar{3}$)	7.30	8.18	9.63	0.01	(0.08)	0.57
$^{125}Te^+_{Si}$						
$^{125}Te^+$	1034	1133	3492	0.0	0.0	0.0
Si(1,1,1)	0.9	5.14	17.7	2.5	2.8	9.8
Si(2,2,0)	< 0.001	3.64	5.26	0.02	(0.06)	0.21

a small s admixture only [except for the Si(3,3,$\bar{3}$) ligand where the p-type wave function is essentially zero]. The main effect of the valence-band polarization is to add some s-type spin density to the predominantly p-type spin density.

Since the total spin of a paramagnetic chalcogen impurity must obey a sum rule the extra spin density supplied by the valence-band polarization (which in our calculations was found to be positive at all ligands considered) must be balanced by a negative contribution at more distant ligands. It is therefore possible that this negative contribution at some ligand is larger than the (positive) contribution of the single-particle wave function in which case the total spin density could turn out to be negative at this ligand. We have not been able to observe this effect due to computational limitations. Our calculations are limited to the four silicon ligand shells given in Table III. Although the magnitude of the HFI is not a monotonous function of the distance we find our calculations cover most of the larger contact and dipolar HFI constants found experimentally. In fact, for S^+_{Si} and Se^+_{Si} only four shells with larger HFI matrix elements are found in the experiment for which there is no counterpart in our calculation.

TABLE IV. Contributions to the contact hyperfine interaction from the single-particle state in the gap, the ns core states, and the valence band, respectively, for the chalcogen point defect and the Si ligands.

	Chalcogen	Si(1,1,1)	Si(2,2,0)	Si(3,1,$\bar{1}$)	Si(3,3,$\bar{3}$)
S^+_{Si}					
gap state	239.3	21.1	< 0.001	3.0	6.0
1s	2.5	−3.9	−0.13	−0.04	0.00
2s	−0.6	−0.2	−0.23	−0.05	0.00
valence band	−0.7	14.9	6.00	0.20	0.18
total	240.5	31.9	5.64	3.11	6.18
Se^+_{Si}					
gap state	1176	15.6	< 0.001	2.66	7.30
1s	6.23	−3.1	−0.12	−0.03	0.00
2s	1.59	−0.3	−0.19	−0.04	0.00
3s	−3.55				
valence band	28.5	13.3	5.60	0.16	0.88
total	1208	25.5	5.29	2.75	8.18

Even with the present state of agreement between the experimental and theoretical data the assignment of experimental numbers to shells for which we have theoretical data is not in all cases unambiguous. It seems clear that the Si(1,1,1) and Si(3,3,$\bar{3}$) are to be assigned to the two largest HFI interactions in the experiment for which a [111] shell symmetry was found. For the experimental data for which a [110] shell symmetry was found there is one shell with an isotropic constant which is larger by more than about a factor of 2 compared to the others. The similarity with our theoretical data strongly suggests that this should be due to the nearest ligand shell (2,2,0). The next two (three in the case of Se_{Si}^{+}) experimental contact interactions of [110] shell symmetry which are listed in Table III are of about the same size. For one shell in each impurity system, however, the dipolar HFI is of the order of 0.5 MHz, while for the remaining shells this quantity is smaller by a factor of about 7. From the order of magnitude of the theoretical dipolar HFI we tentatively assign the (3,1,$\bar{1}$) shell to the experimental data for which the dipolar HFI is largest. Inspection of Table III shows that the dipolar HFI is also not a monotonous function of the ligand shell distance.

For the S_{Si}^{+} and Se_{Si}^{+} point defects the comparison of the single-particle contribution a_l of the contact interactions at the Si ligands with the experimental data shows that a simple single-particle LCAO analysis of experimental data is usually not meaningful. For shallow donors in Si which are described by the effective mass theory (EMA) (see Refs. 27 and 26) the spin density at the nearest-neighbor ligand is small because there is a node in the single-particle wave function. The deep-level single-particle wave function also is oscillatory as can be seen from the fact that the contribution a_l of the single-particle wave function to the contact term for the Si(2,2,0) ligand is virtually zero while this contribution for the Si(3,3,$\bar{3}$) ligand is larger by a factor of 2.5 than the corresponding value for the much closer Si(3,1,$\bar{1}$) ligand. The same features are found for S, Se, and Te in all charge states.

For interstitial chalcogen point defects we find a bound state in the gap that transforms according to the t_2 irreducible representation. The contribution from the single-particle wave function to the contact interaction at the impurity nucleus is therefore zero. A dynamical Jahn-Teller effect could in principle remove this conflict with the experimental data but is unlikely. Furthermore, the large dipolar interaction (calculated to be 230 MHz for Se_{int}^{+}, for example) has not been observed in the magnetic resonance experiments. We therefore can conclude that the paramagnetic centers observed experimentally cannot be identified with interstitial chalcogen point defects.

B. Chalcogen pairs

We have calculated the total energies for pairs of identical chalcogen atoms where both chalcogen atoms are either at substitutional sites (SS), or at interstitial sites (II) and for pairs for which one chalcogen is at a substitutional site and the other is at an interstitial site (SI). For the former two pairs the symmetry is D_{3d} which is also suggested from ENDOR data.[14] The SI pair has C_{3v} symmetry. For the D_{3d} pairs we have studied two different configurations: in the first (NN) configuration both chalcogen sites are at a nearest-neighbor distance separated by the distance vector d (1,1,1,), while in the second (NNN) configuration both impurities have the same symmetry but are separated by d (3,3,3). For the NNN SS pairs the two chalcogen atoms are separated by two "empty" spheres along the [111] direction while for the NNN II pair the impurities are separated by two Si ligands.

If we compare both pairs we have to bear in mind an important distinction between the NN and the NNN pair: the NNN pair can be understood as a "molecule" of two interacting point defects, each consisting of a chalcogen atom held in place by the four dangling bonds of a vacancy. The NN pair in contrast can be represented in the corresponding picture by a chalcogen molecule situated in a divacancy where it interacts with six dangling bonds. While in the former case the electronic states can be interpreted as the bonding-antibonding combinations of the corresponding states of the two point defects this is not true for the NN pair.

For the SS Se pairs the induced densities of states transforming according to the A_1 representation is shown in Fig. 5 both for the NN and NNN configuration. The induced density of states for the NNN pair is in many respects similar to the induced density of states for the isolated point defect. Note however that states transforming according to the T_2 representation in a system of T_d point-group symmetry split into states transforming according to A_1 and E in a C_{3v} environment. We, therefore, find a remainder of the T_2 representation of the isolated point defect in the A_1 peak near -5 eV for the NNN pair. The states below the valence band as well as the superdeep states near -7.5 eV are the even-odd combinations of the corresponding states of isolated point defects. The same applies for the deep levels above the valence band for the NNN pair. These can be understood as the antibonding combination of the impurity s states and the ligand p states. For the pair we have two A_1 deep levels which for the neutral charge state are fully occupied. Depending on the position of the Fermi level these give rise to two different paramagnetic states.

The induced density of states for the NN SS pair shows a marked difference to the case of a NN pair in Fig. 5. The peak near -8 eV has a different origin than the two peaks at the same energy for the NNN pair. It is caused by the bonding combination of the $\sigma_g(p)$ states of the Se molecule with the a_{1g} states of a divacancy (see Ref. 40). The peak near -5 eV is therefore missing. The antibonding combination of the states giving rise to the peak near -8 eV gives rise to the deep level in the gap. There is only the A_{1g} state in the gap. The A_{1u} state arising from the interaction of the $\sigma_g^*(p)$ state of the Se

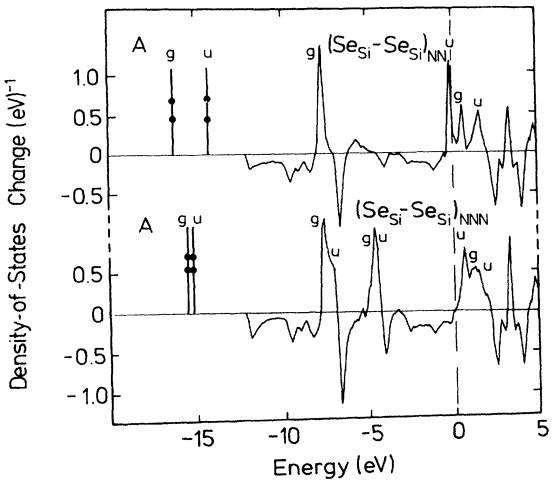

FIG. 5. Induced density of states transforming according to the A_{1g} and A_{2u} representations for the $(Se_{Si}\text{-}Se_{Si})^+$ NN pair (upper panel), and for the $(Se_{Si}\text{-}Se_{Si})^+$ NNN pair (lower panel).

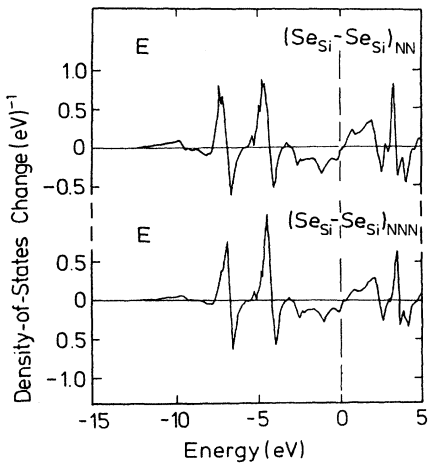

FIG. 6. Induced density of states transforming according to the E representation for the $(Se_{Si}\text{-}Se_{Si})^+$ NN pair (upper panel), and for the $(Se_{Si}\text{-}Se_{Si})^+$ NNN pair (lower panel).

molecule with the a_{2g} state of the divacancy is found at the top of the valence band.

While the density of induced states transforming according to the A_1 representation for both species of pairs is very similar for Se-Se and S-S pairs, there is a marked difference to the Te-Te pairs: Here the lower a_{1u} state is slightly above the valence band and forms a deep state in the gap. Figure 6 shows the induced density of states transforming according to E representation for the NN and NNN SS pairs. The resonance-antiresonance structures for both systems are virtually identical with little if any changes at all. Induced densities of states for the II NN pair and the SI pairs have been published in Refs. 41 and 40.

1. *Total energies and pair stability*

We list in Table II the electron removal energies for NN and NNN SS pairs. The stability of these pairs is calculated from a comparison of the total energy of the pair in the different charge states with that of two substitutional point defects. This is shown in Figs. 3(b) and in 3(c) for the NN S_{Si}-S_{Si} pair and for the NNN S_{Si}-S_{Si} pair, respectively. Corresponding data for the NN and NNN Se_{Si}-Se_{Si} pairs are shown in Figs. 4(b) and 4(c), respectively. For the neutral NN pairs there is definitely a strong binding of the pairs which, however, is lost completely as the Fermi energy is moved below midgap because of the strong Coulomb repulsion. The neutral NNN pairs, on the other hand, do not bind because these can be regarded as interacting close shell atoms for which we expect a repulsion. The NNN S_{Si}-S_{Si} pair will be bonding if the Fermi energy is near midgap while for the NNN Se_{Si}-Se_{Si} pair the stability is questionable. If we compare the formation energies of NN and NNN SS pairs in Figs. 3(d) and 4(d) we find that the NNN pairs would be more stable for p-type material. Because we have not calculated complete total-energy surfaces we cannot decide if in equilibrium the NNN pairs are stable with respect to NN pair formation and also with respect to separation into point defects.

The Te_{Si}-Te_{Si} pair turned out to be unstable according to our calculations. The geometrical misfit of the larger Te atom in the Si lattice, however, must lead to a significant lattice distortion both for the point defect and for the pairs. Since this effect is not taken into account in our total-energy calculations we do not believe that our calculations can really exclude the stability of SS Te pairs, in particular as for the neutral pair the total energy is by only 0.3 eV larger than twice the energy of the point defect (see Fig. 7).

2. *Hyperfine constants for S_{Si}-S_{Si} and Se_{Si}-Se_{Si} pairs*

The HFI matrix elements that are obtained by our calculations are listed in Table V for the positively charged paramagnetic NN SS pairs and for the singly and threefold positively charged paramagnetic SS NNN pairs. While the results for the NN pairs are essentially identical (except for the calculation of the relativistic contact HFI which is now corrected) with those reported earlier[39] there are marked differences for the NNN pairs. This difference is due to the fact that in the earlier calculations we had ignored the fact that there are two states in the gap, the a_{2u} state at lower energies which for the NN pair was found in the valence band and the a_{1g} state at higher energies. In earlier calculations we used the lower C_{3v} symmetry instead of the full D_{3d} symmetry and obtained a result for the HFI interaction that was the sum

TABLE V. Calculated hyperfine interaction matrix elements (in MHz) for nearest-neighbor SS pairs and for next-nearest [111] SS pairs are compared with experimental data (Ref. 14 for the ligand interactions and for the interactions with the Se nucleus, and Ref. 13 for the interactions with the S nucleus, respectively). There are no experimental data for the Te pairs.

Pair	Chalcogen				Si(1,1,$\bar{1}$)			
	a_l	a_{tot}	b_l	b_{tot}	a_l	a_{tot}	b_l	b_{tot}
$(S_{Si}\text{-}S_{Si})^+$ NN pair	87.1	89.7	1.1	1.4	9.8	13.5	3.4	(3.6)
$(S_{Si}\text{-}S_{Si})^+$ NNN pair	98.5	99.4	0.14	(0.45)	0.071	0.11	0.16	(0.19)
$(S_{Si}\text{-}S_{Si})^{+++}$ NNN pair	1360	140.4	0.71	(2.0)	9.8	10.3	2.5	(3.0)
expt.		115.3		0.878		23.85		4.875
						11.834		0.428
						8.441		0.460
$(Se_{Si}\text{-}Se_{Si})^+$ NN pair	408.3	414.4	6.78	7.61	9.34	11.7	3.0	(3.2)
$(Se_{Si}\text{-}Se_{Si})^+$ NNN pair	344.0	378.0	0.93	(3.8)	≤ 0.001	1.40	0.11	(0.35)
$(Se_{Si}\text{-}Se_{Si})^{+++}$ NNN pair	595.0	597.0	0.64	(1.02)	0.81	0.96	0.34	(0.37)
expt.		606.7		5.566		21.69		5.44
						12.675		0.471
						8.228		0.442
$(^{125}Te_{Si}\text{-}^{125}Te_{Si})^+$ NN pair	364.0	458.0	1.94	3.00	1.00	7.11	0.58	0.81
$(^{125}Te_{Si}\text{-}^{125}Te_{Si})^{+++}$ NN pair	1439.0	1445.0	86.7	94.5	2.01	4.9	1.30	1.36

of the contributions of both states. We list in the table results for the HFI interaction at the chalcogen nucleus and also at the nearest Si(2,2,0) ligand (for the pairs the distance vectors to the nearest chalcogen nucleus of the pair is given). Also listed in Table V are experimental data[14,13] for the HFI interaction matrix elements at the chalcogen nucleus and at the Si ligands with (1,1,0) orientation with respect to the pair oriented in the [111] direction. Again from the experimental data alone it is unknown which measured interaction matrix element belongs to the calculated result of the NN Si(1,1,$\bar{1}$) neighbor shell. We, therefore, list the three experimental values of [110] shell ligands with the largest HFI contact interaction (which are also the largest dipolar interaction matrix elements).

A comparison of the HFI contact interaction data at the chalcogen nuclei with those of the point defects shows that the magnitude is decreased by about a factor of 3. A factor of 2 would be expected because the paramagnetic spin is shared by the two chalcogen impurities, the extra reduction shows that the electronic state of the pair is different from that of a point defect. Inspection of the spin density distribution (see Table I) for the NN SS pairs shows the following.

(1) The s-like spin density located in the impurity ASA sphere is approximately equal to the sum of p-like and d-like contributions.

(2) If we compare the total spin density in the chalco-

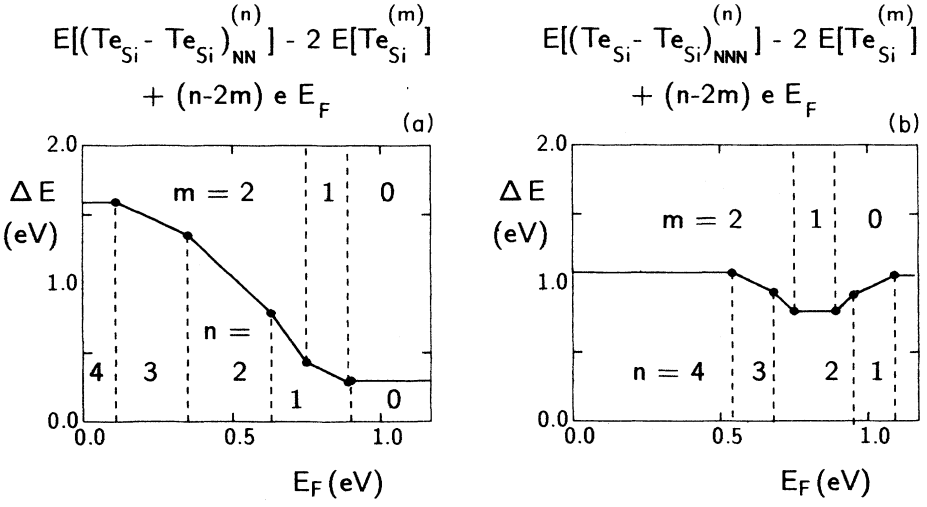

FIG. 7. Formation energy of substitutional Te defect clusters in different configurations and charge states as a function of the Fermi energy: (a) difference between a NN pair and two point defects; (b) difference between a NNN pair and two point defects.

gen ASA sphere of a point defect with that of the two chalcogens of the pair we find 70% more spin density for the pair, although we count the spin density of the upper a_{1u} state only. This shows that one has to be careful not to take the smaller contact term of the pair state alone as a measure of the spin density.

(3) If we compare the spin densities at the nearest-neighbor Si ligands we do not find a significant difference between the NN pair and the point defect. This indicates that although the a_{1g} state of the pair is not as deep as the a_1 state of the point defect the spin density is *not* more delocalized than that of a point defect.

If we identify the paramagnetic pair found experimentally with the calculated data for the NN SS pair we find a rather good agreement for the contact interactions at the chalcogen atom. The dipole interaction matrix elements at the same nucleus come out somewhat too large. For the Si(1,1,$\bar{1}$) ligand we have listed three different experimental sets of data. From the similarity of the numbers for the contact term one might be tempted to identify the Si(1,1,$\bar{1}$) ligand data with the second line of the experimental data. Closer inspection, however, shows that this choice is in fact incompatible with our calculations: a fit to the experimental data would require that the p-like spin density in the Si(1,1,$\bar{1}$) shell (about 1.5% of the total spin) is reduced by a factor of 9. We explain the discrepancy between experimental and calculated data by the assumption that the s-like contribution, which with 0.1% of the total spin turns out to be rather small in the Si(1,1,$\bar{1}$) sphere, comes out to be too small in the calculations.

For the NNN pairs we have two distinct localized states in the gap for which we obtain HFI matrix elements which are markedly different, in particular for the Si(1,1,$\bar{1}$) ligands. These states do not seem to have been observed experimentally although at least for the NNN S-S pair we find a wide range of stability. Greulich-Weber, Niklas, and Spaeth[14] have given an argument which shows that the pair observed in their ENDOR experiment cannot be in the II configuration. The same argument can be used to exclude the possibility that they measured the NNN SS pair: in both cases one should have observed a HFI interaction which belongs to a Si ligand in the [111] direction. No such ligand has been observed in the ENDOR experiments. This fact is compatible only with our calculations if the pairs observed in ENDOR are in the NN SS configuration.[39]

We also list in Table V the calculated HFI matrix elements for the two states of the Te-Te SS NN pair. Unfortunately there are no experimental data available for these states and, as mentioned before, the existence of these pairs is questionable.

IV. CONCLUSIONS

Formation energies, electron removal energies, and hyperfine fields are calculated using the LMTO-ASA Green-function method. One of the main advantages of this paper is that all these quantities are evaluated with the same self-consistent calculation. In addition, the use of the LMTO-ASA scheme is especially appropriate for the calculation of the HFI constants because (1) the contributions to the HFI matrix elements arising from the single-particle wave function of the gap state, the polarization of the valence-band states, and the polarization of the different core states can be calculated within the same formalism; (2) the use of a basis that is centered at the nuclei simplifies the calculation of the HFI matrix elements and their interpretation.

One of the main problems with the interpretation of experimental ligand hyperfine data is that from the data alone only the symmetry type of the shells but not the distance with respect to the defect center can be deduced. We have shown in this work that the simultaneous calculation of formation energies and HFI constants makes it possible to discriminate between ligand shells of the same symmetry.

Besides the local-spin-density approximation for the exchange-correlation functional, there is some uncertainty of the results due to the neglect of lattice relaxation. We feel, however, that for substitutional S and Se defects this approximation is justified and does not alter the principal conclusions for chalcogen impurities.

We find that the contributions from the spin polarization of the valence band to the contact HFI matrix elements are relatively unimportant *at the chalcogen nuclei.* At the nearer Si ligand nuclei these contributions, however, sometimes are larger than the contribution arising from the single-particle wave function of the deep state. This shows that an interpretation of the experimental data in terms of a single-particle LCAO spin density can lead to incorrect estimates about the bonding properties and about the localization of the wave functions.

As in the case of shallow donors in Si we find that the single-particle wave function of the deep level does not decay exponentially but oscillates and produces nodes. For deep levels the single-particle wave function is of course quite different from that of a shallow donor: For a shallow donor the nearest-neighbor ligand nucleus is virtually at a node of the wave function while for chalcogen point defects the next-nearest Si(2,2,0) ligand nucleus is at the node. The oscillatory nature of the wave function is borne out by the fact that the contact HFI for the Si(3,3,$\bar{3}$) ligand is about twice the value for the Si(3,1,$\bar{1}$) ligand which is much nearer to the impurity. In contrast to the case of shallow donors in Si, the total spin density is much more localized around the impurity site, but much less than indicated by the single-particle wave function. Compared with the valence-band polarization the core polarization only plays a minor role for the chalcogen impurities in Si. However it is of some importance at the nearest Si(1,1,1) neighbor where it contributes about 20% of contribution due to the single-particle wave function.

From the results of the total-energy calculation we in-

fer that chalcogen point defects will be built in as substitutional point defects with the possible exception that the S impurity in n-type Si might also be found at an interstitial position. A comparison of the calculated HFI data with experimental data convincingly proves that all paramagnetic chalcogen point defects in tetrahedral positions are at a substitutional site. Interstitial point defects would show a Jahn-Teller distortion and hence no tetrahedral symmetry. Even if the distortion would turn out to be small the hyperfine data would be drastically different from those found experimentally. The paramagnetic resonance data of the EPR and ENDOR experiments are, therefore, compatible only with our results for substitutional point-defect sites and here the agreement between experiment and theory is convincing.

For the defect pairs we also find that both chalcogens will be built in at substitutional positions. From the agreement with experimental HFI data we conclude that for the paramagnetic pairs found experimentally[8,10–14] the chalcogen atoms must have been in nearest-neighbor positions. Our total-energy calculations also indicate a range of (admittedly weak) stability for a pair with D_{3d} symmetry for which the chalcogens are separated by three nearest-neighbor distances. It is not clear if these pairs can be identified with the chalcogen (X) defects reported in infrared absorption experiments (see, e.g., Wagner *et al.*[1]). A convincing identification probably can be made only if these defect states are observed in magnetic resonance experiments.

ACKNOWLEDGMENTS

The authors are grateful to Dr. Gábor Corradi for his help during the numerical calculations and to Andreas E. Kumm for the implementation of the core polarization program. Financial support from the Deutsche Forschungsgemeinschaft is thankfully acknowledged.

[1] P. Wagner, C. Holm, E. Sirtl, R. Oeder, and W. Zulehner, in *Festkörperprobleme, Advances in Solid State Physics*, edited by P. Grosse (Vieweg, Braunschweig, 1984), Vol. 25, p. 191.
[2] W. E. Krag and H. J. Zeiger, Phys. Rev. Lett. **8**, 485 (1962).
[3] J. C. Swartz, D. H. Lemmon, and R. N. Thomas, Solid State Commun. **36**, 331 (1980).
[4] H. G. Grimmeiss and B. Skarstam, Phys. Rev. B **23**, 1947 (1981).
[5] E. Sirtl, in *Defects in Silicon*, edited by L. C. Kimerling and M. Bullis (The Electrochemical Society, Pennington, NJ, 1983).
[6] E. Janzén, R. Stedmann, G. Grossmann, and H. G. Grimmeiss, Phys. Rev. B **29**, 1907 (1984).
[7] S. D. Brotherton, M. J. King, and G. J. Parker, J. Appl. Phys. **52**, 4649 (1981).
[8] G. W. Ludwig, Phys. Rev. **137**, A1520 (1965).
[9] W. E. Krag, W. H. Kleiner, H. J. Zeiger, and S. Fischler, J. Phys. Soc. Jpn. Suppl. **21**, 230 (1966).
[10] H. G. Grimmeiss, E. Janzén, H. Ennen, O. Schirmer, J. Schneider, R. Wörner, C. Holm, E. Sirtl, and P. Wagner, Phys. Rev. B **24**, 4571 (1981).
[11] S. Greulich-Weber, J. R. Niklas, and J.-M. Spaeth, J. Phys. C **17**, L911 (1984).
[12] P. Wörner and O. F. Schirmer, Solid State Commun. **51**, 665 (1984).
[13] A. B. van Oosten and C. A. J. Ammerlaan, Phys. Rev. B **38**, 13 291 (1988).
[14] S. Greulich-Weber, J. R. Niklas, and J.-M. Spaeth, J. Phys. Condens. Matter **1**, 35 (1989).
[15] H. P. Hjalmarson, P. Vogl, D. J. Wolford, and J. D. Dow, Phys. Rev. Lett. **44**, 810 (1980).
[16] S. Y. Ren, W. M. Hu, O. F. Sankey, and J. D. Dow, Phys. Rev. B **26**, 951 (1982).
[17] O. F. Sankey and J. D. Dow, Solid State Commun. **51**, 705 (1984).
[18] R. W. Jansen and O. F. Sankey, Phys. Rev. B **33**, 3994 (1986).
[19] G. Kim, J. D. Dow, and S. Lee, Phys. Rev. B **40**, 7888 (1989).
[20] U. von Barth and L. Hedin, J. Phys. C **5**, 1629 (1972).
[21] R. O. Jones and O. Gunnarsson, Rev. Mod. Phys. **61**, 689 (1989).
[22] O. Gunnarsson, O. Jepsen, and O. K. Andersen, Phys. Rev. B **27**, 7144 (1983).
[23] M. Scheffler, Physica B+C **146B**, 176 (1987).
[24] J. R. Niklas and J. M. Spaeth, Solid State Commun. **46**, 121 (1983).
[25] E. B. Hale and R. L. Mieher, Phys. Rev. **184**, 739 (1969).
[26] J. L. Ivey and R. L. Mieher, Phys. Rev. B **11**, 822 (1975); **11**, 1955 (1975).
[27] E. B. Hale and R. L. Mieher, Phys. Rev. **184**, 751 (1969).
[28] J. Noffke and H. Gollisch, Phys. Rev. B **32**, 7148 (1985).
[29] B. D. Dunlap and G. M. Kalvius, in *Mössbauer Isomer Shifts*, edited by G. K. Shenoy and F. E. Wagner (North-Holland, Amsterdam, 1978), p. 15.
[30] A. J. Freeman and D. E. Ellis, in *Mössbauer Isomer Shifts* (Ref. 29), p. 111.
[31] S. Blügel, H. Akai, R. Zeller, and P. H. Dederichs, Phys. Rev. B **35**, 3271 (1987).
[32] G. Breit, Phys. Rev. **35**, 1447 (1930).
[33] F. Beeler, M. Scheffler, O. Jepsen, and O. Gunnarsson, Phys. Rev. Lett. **54**, 2525 (1985).
[34] W. Shockley and J. T. Last, Phys. Rev. **107**, 392 (1957).
[35] W. Shockley and J. L. Moll, Phys. Rev. **119**, 1480 (1960).
[36] W. Gebhardt, in *Festkörperprobleme IX*, edited by O. Madelung (Vieweg, Braunschweig, 1969), p. 99.
[37] M. J. Caldas, J. Dabrowski, S. Fazzio, and M. Scheffler, Phys. Rev. Lett. **65**, 2046 (1990).
[38] H. Overhof, M. Scheffler, and C. M. Weinert, Mat. Sci. Forum **38-41**, 293 (1989).
[39] H. Overhof, M. Scheffler, and C. M. Weinert, Mat. Sci. Eng. **4**, 315 (1989).
[40] C. M. Weinert and M. Scheffler, Phys. Rev. Lett. **58**, 1456 (1987).
[41] C. M. Weinert and M. Scheffler, Mat. Sci. Forum **10-12**, 25 (1986).